Exploring two regimes of water mobility in unsaturated expansive clay using NMR relaxometry

Pablo Eizaguirre, Anh Minh Tang, Benjamin Maillet, Rahima Sidi-Boulenouar, Jean Talandier, Jean-Michel Pereira, Minh Ngoc Vu, Baptiste Chabot, Patrick Dangla, Michel Bornert, et al.

Applied Clay Science 251 (2024) 107324

Contents lists available at ScienceDirect

Applied Clay Science

journal homepage: www.elsevier.com/locate/clay

Research Paper

Exploring two regimes of water mobility in unsaturated expansive clay using NMR relaxometry

Pablo Eizaguirre [a,b], Anh Minh Tang [a,*], Benjamin Maillet [a], Rahima Sidi-Boulenouar [a], Jean Talandier [b], Jean-Michel Pereira [a], Minh Ngoc Vu [b], Baptiste Chabot [a], Patrick Dangla [a], Michel Bornert [a], Patrick Aimedieu [a]

[a] Navier Laboratory, Ecole des Ponts, Univ Gustave Eiffel, CNRS, Marne-la-Vallée, France
[b] French National Radioactive Waste Management Agency (Andra), Châtenay-Malabry, France

ARTICLE INFO

Keywords:
Low field ^{1}H NMR
Relaxation times
Surface limited relaxometry
Adsorbed water
Expansive clay
Water retention

ABSTRACT

The hydration behaviour of unsaturated expansive clays, crucial for applications such as radioactive waste management, remains a challenging and incompletely understood phenomenon given the complexity of characterizing their pore network dynamics upon water absorption. The evolution of porewater populations, distinguished as immobile adsorbed water attached to the clay particles surface and capillary water, presumably governs the kinetics of water mobility in wetting or drying processes.

Nuclear Magnetic Resonance (NMR) relaxometry experiments have reported the increase of water mobility during the wetting process of expansive clays but the evolution of water populations remained unidentified. This study presents relaxation time distributions and relaxation time maps found for a bentonite/sand mixture (with Na-montmorillonite) at various relative humidities, reproducing its hydration. Valuable insights into particular experimental procedure, data-treatment and interpretation for expansive clay are provided. Relaxation times in Na-montmorillonite highlighted a two-regime evolution as a function of water content, in accordance to models, featuring the properties of adsorbed water, which is considered fully dominant during the first regime (relative humidity lower than 90%).

An empirical model reproducing the two-regime dependance of water content on relaxation times was proposed. Moreover, a new formulation enabled quantifying the adsorbed water fraction in expansive clay from relaxation time measurements. Finally, the porewater populations were quantified for Na-montmorillonite as a function of water content, demonstrating strong agreement with supercooling observations in freezing experiments.

1. Introduction

The hydration of unsaturated expansive clay has not yet been completely understood, even though it has been a focus of investigations in the past 40 years. Particularly,the use of expansive clay as buffer material in the radioactive waste management industry demands to precisely characterize and predict via appropriate models its long-term hydration (Gens et al., 2002; Lloret et al., 2003; Sellin and Leupin, 2013) characterized by very slow water transfer. Hydration processes may potentially take hundreds or several thousands of years to reach hydraulic equilibrium at in situ conditions.

Water transfer in unsaturated soils depends on the amount and connectivity of water in the pore network. Given the wide pore size distribution of compacted clay mixtures (from approximately 1 nm to hundreds of μm) and the complexity of the electro-chemical interactions between water and the clay particles (hydrogen bonding, hydration of exchangeable cations, osmotic attraction by Stern layer and diffuse double layer, charged surface–dipole attraction, London dispersion forces attraction and capillary condensation) (Low, 1961; Madsen and Müller-Vonmoos, 1989; Wersin et al., 2004; Leroy and Revil, 2004; Mitchell and Soga, 2005), it is expected that different porewater populations may coexist and develop complex dynamics during wetting/drying processes. In practice, porewater populations have been classified as a function of their expected mobility as: capillary water (with advective mobility) and adsorbed water (less mobile water due to its strong electro-chemical interaction with the clay minerals). The water

* Corresponding author at: Ecole des Ponts ParisTech, Laboratoire Navier/Géotechnique, 6-8 avenue Blaise Pascal, 77455 Marne-La-Vallee, France.
E-mail address: anh-minh.tang@enpc.fr (A.M. Tang).

https://doi.org/10.1016/j.clay.2024.107324
Received 16 October 2023; Received in revised form 26 February 2024; Accepted 26 February 2024

population featuring boiling temperatures above 315 °C is often called structural water and is assumed to be completely static. Hence, it would not contribute to water transfer and it is not considered as porewater in this study. Adsorbed water features supercooling properties, a higher density (1.20–1.30 Mg/m^3) at low relative humidity (*RH*) (Martin, 1960; Jacinto et al., 2012; Bahramian et al., 2017; Wang et al., 2020; Navarro et al., 2022) and its transfer in porous media is presumably governed by water vapour diffusion. Several studies based on water retention models concluded that adsorbed water is predominant in clay soils with low *RH* whereas at high *RH* adsorbed water and capillary water coexist, being this evolution very impactful on the unsaturated hydraulic conductivity of clays (Tuller et al., 1999; Tuller and Or, 2005; Lebeau and Konrad, 2010; Revil and Lu, 2013; Navarro et al., 2015; Dieudonne et al., 2017). Capillary water might appear when connectivity between the porewater matrix is reached, attributing mobility to the porewater matrix. Thus, two different regimes of mobility are expected depending on the *RH* in the soil.

The quantification of capillary and adsorbed water populations in unsaturated clays could be better demonstrated by experiments on microstructural quantification of water populations, independently from water retention models. The aim of this study is to characterize the two-regime water mobility evolution from NMR (Nuclear Magnetic Resonance) relaxometry tests providing useful experimental data, a practical empirical model that could reproduce the experimental results and the quantification of adsorbed and capillary water in a wetting process.

1.1. Nuclear magnetic resonance relaxometry

Dynamic low-field NMR relaxometry has been proved as a useful non-invasive tool for measuring liquid transfers, water mobility (depending on pore size, adsorption and paramagnetic component) and porewater quantification in porous media through the investigation of longitudinal (T_1) and transversal (T_2) relaxation time distributions obtained by IR (Inverse Recovery) and CPMG (Carr-Purcell-Meiboom-Gill) NMR sequences, respectively (Gao and Li, 2015; Maillet et al., 2022; Catinat et al., 2023). The technique is based on the principle that certain atomic nuclei possess a property called "nuclear spin," which generates a magnetic moment. When placed in a strong magnetic field and exposed to radiofrequency pulses, these nuclei can absorb and reemit energy at specific frequencies, resulting in a resonance phenomenon. The return to equilibrium of the magnetization (absence of resonance) is defined by the T_1 and T_2 which are influenced by the mobility, paramagnetism and configuration of surrounding macromolecules due to proton exchange (chemical exchange).

Regarding compacted expansive clay, NMR relaxometry experiments do not exhibit directly distinctive responses from each of its porewater populations, contrary to other soils (Jaeger et al., 2009). Hence, T_1 and T_2 are presumably the weighted average response of all porewater populations due to a fast diffusion exchange between them (Fleury et al., 2022). Investigations involving CPMG tests during freezing experiments in Na-montmorillonite determined the adsorbed water fraction at four unsaturated states by the supercooling effect (Fleury et al., 2013). Similarly, a gas hydrate formation test followed by CPMG in montmorillonite at different hydric states demonstrated that hydrate formation occurs at water contents above 15% when the binding strength of water molecules is progressively lower (Sun et al., 2021). Several descriptions of porewater in expansive clay have been provided by interpretation of NMR relaxometry tests using the Surface Limited Relaxometry theory (described in Section 4.4.1) with the support of porosity analysis from microstructural observations such as X-Ray Diffractometer (Ohkubo et al., 2008, 2021; Fleury et al., 2013; Rongwei and Tsukahara, 2020), Mercury Intrusion Porosimeter (Ma et al., 2020; Tian and Wei, 2020; Tian et al., 2023) or other experimental techniques such as SAXS (Muurinen et al., 2013).

2. Materials and method

2.1. Compacted bentonite/sand mixture

The experimental campaign was performed on a compacted mixture of granular WH2 gelclay bentonite from Wyoming (USA) and quartz sand. This material is being considered as candidate material for the engineered barrier system in the "Cigéo" project of Andra (French National Agency for Radioactive Waste Management) for geological high-level radioactive waste disposal. The proportions in dry mass are 40/60 (bentonite/sand), defining $B = 40\%$ as the mass proportion of bentonite in the bentonite/sand mixture. The bentonite featured a particle density of 2.77 Mg/m^3. Based on reported observations on MX80 bentonite from Wyoming (Karnland et al., 2006), the bentonite presented a sodium Na^+ governed cation exchange capacity of 71–88 meq/100 g and a montmorillonite content c_{mmt} of 81.4±2.2%. Mineralogical reports (Table 1) suggested the presence of other minor mineral phases. The sand is a quartz sand with a particle density of 2.65 Mg/m^3. The granulometric curves of both materials were obtained by dry sieving (following the norm AFNOR 1996, NF P94–056) determining the mean grain diameters 0.90 mm and 0.55 mm for the bentonite and the sand, respectively.

A brick (300 × 200 × 100 mm^3) compacted from this bentonite/sand mixture was provided by Andra. It had been pre-compacted at 80 MPa within an industrial process. The dry density of the brick was 2.03 Mg/m^3. In the laboratory, the brick with a gravimetric effective montmorillonite water content, hereafter just named water content w, of 21.0% calculated by Eq. (1), was stored inside sealed plastic bags to avoid moisture exchange with the environment. In addition to the unsaturated samples, a saturated sample was prepared by compacting in the laboratory a sample to a target dry density of 1.86 Mg/m^3 with an initial $w = 16.3\%$. The vertical compaction pressure applied was 60 MPa and the final dimensions without load were 11.1 mm of height and 50 mm of diameter. Only a piece of 12 mm of diameter and 11.1 mm of height cut from the saturated sample was used in the experiments.

$$w = \left(\frac{mass\ of\ water}{dry\ mass\ of\ the\ mixture}\right)\frac{1}{B\ c_{mmt}} \quad (1)$$

2.2. Wetting process

Eight cylindrical samples, with maximum dimensions of 10 mm in height and 12 mm in diameter, in order to fit the spectrometer limits of the NMR device, were manually cut and shaped from the bentonite/sand brick provided by Andra with an initial $w = 21.0\%$. Dry mass of each sample was obtained by oven drying at 105 °C for 24 h at the end of each experiment (Table 2). Dry mass varied slightly because it was difficult to obtain regular cylindrical samples with manual preparation. Each sample was inserted in a porous rigid cylindrical cell having internal dimensions of 12 mm in diameter and 10 mm in height prior to being subjected to a *RH*-controlled environment by using the vapour equilibrium technique (Tang and Cui, 2005) until the mass of the samples (measured every week) was equilibrated with a tolerance of 0.01 g

Table 1
Main phases of the mineralogical composition of a commercial bentonite from Wyoming (USA) (Karnland et al., 2006).

Mineral phase	Weight content (%)
Montmorillonite	81.4
Tridymite	3.8
Plagioclase	3.5
Muscovite	3.4
Quartz	3.0
Gypsum	0.9
Cristobalite	0.9
Illite	0.8
Others	2.3

Table 2
Samples used for NMR measurements. Water retention and relaxometry results.

Solution	Relative Humidity (%)	Dry mass of soil sample (g)	Water content, w (%)	T_1 (ms) (a)	T_2 (ms) (a)	T_2 (ms) (b)
K_2CO_3	44	1.69	15.9	0.58	0.19	0.17
$Mg(NO_3)_2$	55	1.75	20.9	0.78	0.21	0.25
$NaNO_2$	66	1.29	20.9	0.80	0.21	0.26
NaCl	76	1.58	23.3	0.89	0.26	0.30
$NaNO_3$	80	1.68	27.0	0.80	0.25	0.30
$(NH_4)_2SO_4$	84	0.55	28.3	0.65	0.23	0.39
KNO_3	94	1.79	30.7	1.11	0.48	0.55
K_2SO_4	97	1.67	36.9	1.51	0.69	0.80
Pure water	100	2.07	52.8	2.87	1.74	2.35

(a) T_1-T_2 (map).
(b) T_2 (distribution).

between two consecutive measurements. Porous rigid cells facilitated the weighing of the samples during the wetting phase without breaking them as well as limited the swelling of the samples.

To prepare the fully saturated sample, demineralized water was injected at a pressure ranging from 200 to 400 kPa using a pressure/volume controller under constant sample volume conditions. Saturation state was assumed after 12 days, when the injected volume of water was above 130% of the pore volume, water inflow rate was found constant at a constant 400 kPa injection pressure and water outflow could be observed at the side opposite to the water inlet.

2.3. NMR relaxometry measurements

The instrumentation used in the relaxometry experiments was a Bruker low-field NMR Minispec mq20, operating at 0.5 Tesla and a frequency of 20 MHz. The system's detection capabilities are constrained to a cylindrical region with 16 mm diameter and 10 mm height. Beyond this height, signal intensity experience a significant attenuation due to field inhomogeneities, eventually leading to signal loss.

A bi-dimensional sequence IR-CPMG was used to have access to contour maps corresponding to the signal as a function of both T_1 and T_2 simultaneously. In order to have a scanning time of 90 min, the IR measured 60 inversion times logarithmically distributed from 0.16 ms to 1000 ms, while the CPMG measured 60 echoes logarithmically distributed from 0.06 ms to 100 ms. The recovery time was set to 1200 ms. Each inversion was measured 64 times to optimize the signal-to-noise ratio.

T_2 was obtained from measurements of a Carr-Purcell-Meiboom-Gill (CPMG) sequence composed of a first "π/2" pulse and a series of "π" pulses -echoes- distributed at regular intervals of 0.06 ms, producing 3333 echoes with echo times from 0.06 ms to 200 ms. Each sequence of echoes was repeated 256 times to optimize the signal-to-noise ratio with the time of scanning (10 min). Repetitions were separated by a repetition time of 2 s to get a complete relaxation of all protons.

T_1 was obtained from measures of an IR sequence. 100 inversion times distributed logarithmically from 0.16 ms to 1000 ms were performed. The recovery time between inversions was set to 1000 ms, sufficient time to ensure that the magnetization came back to equilibrium. The number of scans, i.e. repetitions of each inversion, was 64 to optimize the signal-to-noise ratio with time (75 min).

Data recovered from the Minispec was converted to relaxation time distributions after treating it through inverse Laplace transform (Provencher, 1982). Relaxation time distributions are statistical distributions which correspond to the time it takes for hydrogen protons contained in the porewater to come back to equilibrium after being subjected to magnetic pulse while inside a magnetic field with its resonance frequency. In T_1 or T_2 distributions, the captured signal intensity is presented as a function of the relaxation time. The signal intensity is linearly related to the number of hydrogen protons detected by the instrumentation. In order to compare the signal intensity observed in the different specimens, the signal was divided by the dry mass of the corresponding sample. Even though the signal intensity value shape depends on the regularization technique, particularly on the parsimony factor, relative analysis of signal evolution is suitable for interpretation because the position of the peaks and the integral below the peak are not affected (Faure and Rodts, 2008; Penvern et al., 2020).

Single T_1 or T_2 distribution data treatment is more accurate and reliable than T_1-T_2 relaxation time maps, where uncertainties from the calculation of the two-dimensional inverse Laplace could contribute negatively to the determination of relaxation time distributions. Additionally, the measurements performed for single T_1 and T_2 characterization are more refined due to the bigger number of inversion times and echoes, respectively.

To prevent any water exchange during the experimentation, the samples were carefully covered one by one with Teflon film avoiding the contact of the sample with the environment. Each sample was weighed before and after the NMR measurements, verifying that they did not experience any appreciable water exchange, larger than 0.01 g. An operating temperature of 20 °C was set by the NMR device.

3. Experimental results

3.1. T_1-T_2 maps

T_1-T_2 relaxation time maps in Fig. 1 present relaxation times between 0.04 ms and 10 ms in the case of T_1 and 0.06 ms (limit of the device) to 10 ms for T_2. Inside this range, each combination of T_1 and T_2 was related to a given signal intensity reproduced by a color bar, which was normalized to the sample dry mass. The number of hydrogen protons measured by the NMR device relaxing at a T_1 and T_2 value, defined the signal intensity value. The resulted relaxation time maps were observed as a probabilistic distribution function of two independent variables (T_1 and T_2).

At $RH = 44\%$, two sources of signal were situated at $T_1 = 0.5$ ms. The faster source, with a peak value $T_2 < 0.06$ ms presumably represented the structural hydroxyls located on the surface of clay minerals as demonstrated by a D_2O exchange experiment (Fleury et al., 2013). This source was only partially captured as the peak of its contour map was not observed. The second source had a peak value $T_2 = 0.2$ ms and represented the hydrogen protons of the porewater, potentially both populations of water (adsorbed and capillary).

With an increase of RH, the faster source (hydroxyls) progressively disappeared while the slower one (porewater) became more and more significant. The two sources were generally separated except in some cases ($RH = 66\%$ and 84%) where they overlapped. Peaks of T_1 for both sources remained similar and increased progressively during wetting. Peak of T_2 for porewater also augmented during wetting while that for hydroxyls barely rose. The ratio T_1/T_2, reflected the mobility of water (bulk water exhibits $T_1/T_2 = 1$), and progressively approached values close to 1 as illustrated by the approximation towards the dashed line in Fig. 1.

3.2. T_1 NMR relaxation time distribution

Distributions of T_1 (Fig. 2) resulted in single peak distributions which evolved from 0.4 ms to 2.3 ms, progressively increasing the signal intensity during hydration. Porewater and hydroxyls could not be distinguished. Therefore, T_1 distributions were not suitable for interpreting the evolution of porewater dynamics. Additionally, T_1 distributions could be influenced by paramagnetic impurities in the clay.

3.3. T_2 NMR relaxation time distribution

The firsts echoes of the CPMG sequence (0.06 ms and 0.12 ms) were

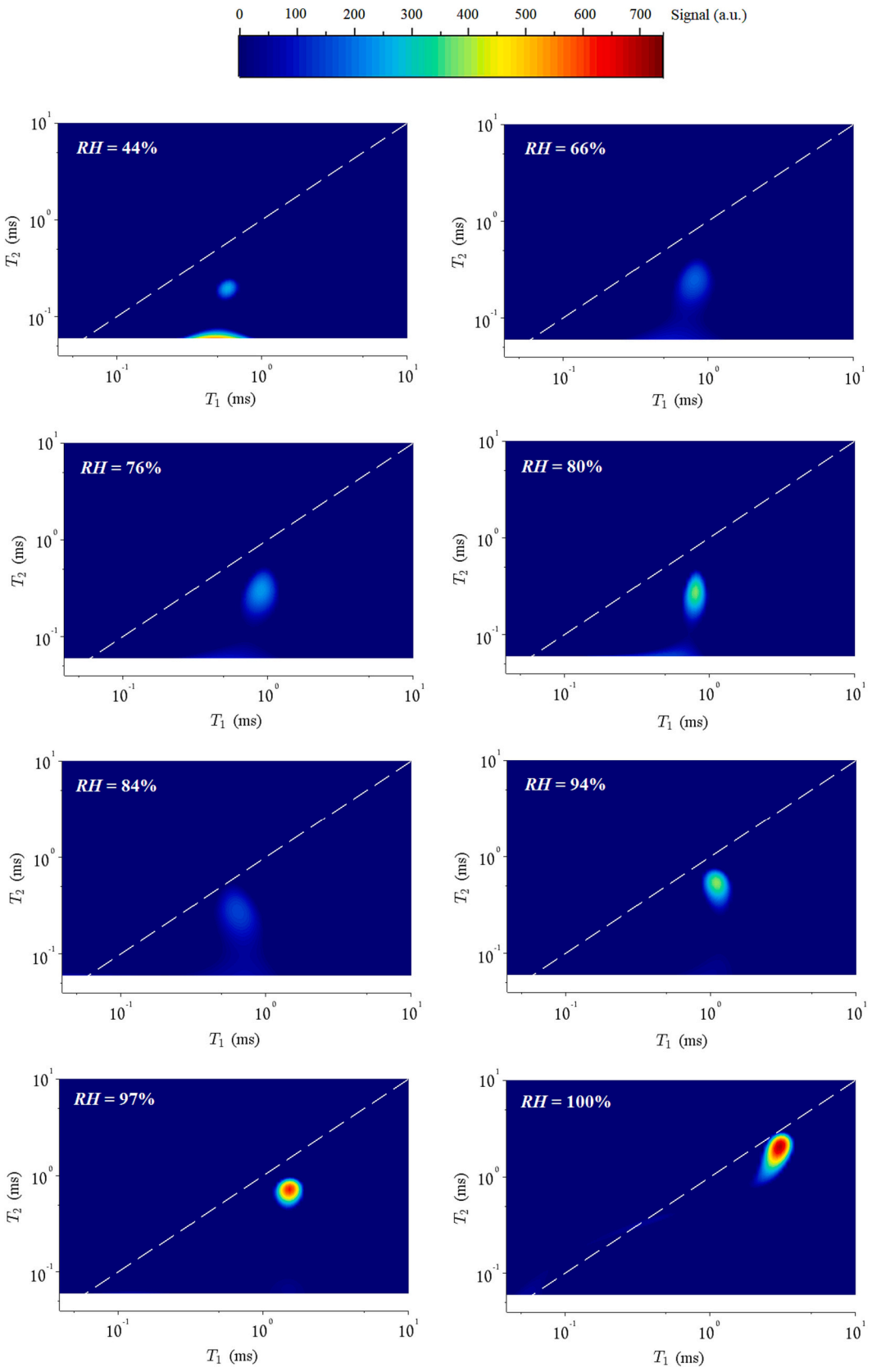

Fig. 1. T_1-T_2 relaxation time maps. Dashed lines represent $T_1/T_2 = 1$.

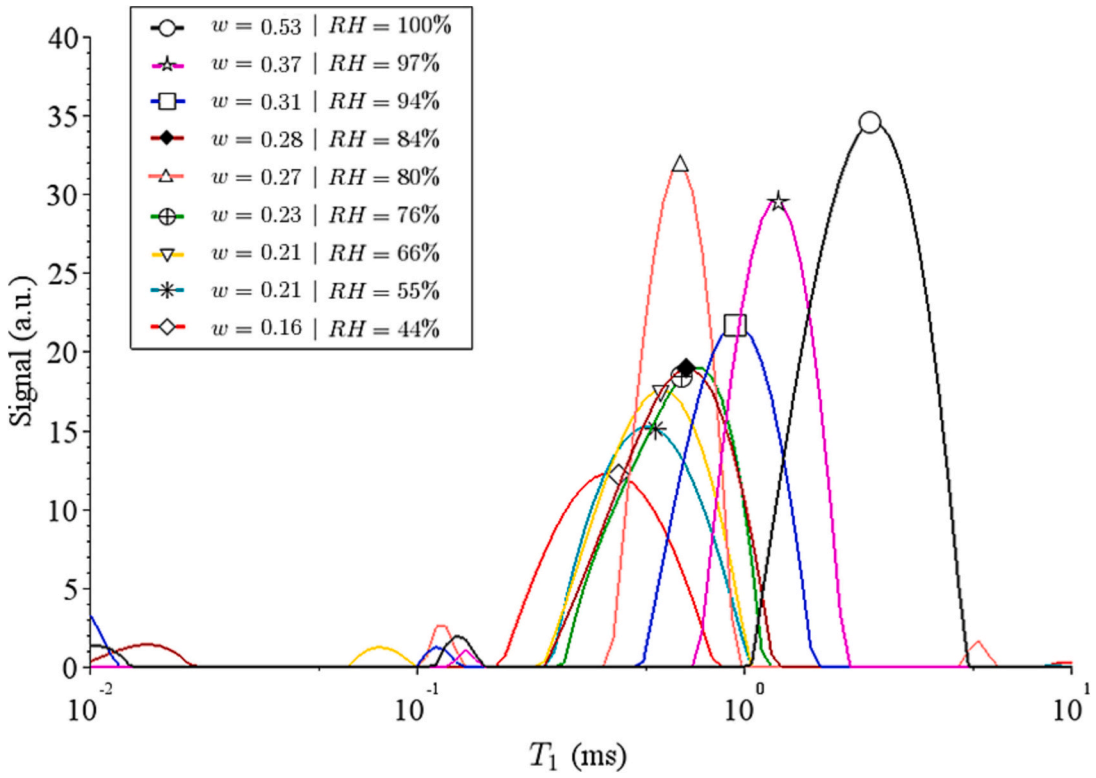

Fig. 2. T_1 distribution. The statistically most representative relaxation time of each peak (characteristic T_1) has been represented with a point symbol in the distribution.

sensitive to the signal originated by the hydroxyls according to the T_1-T_2 relaxation time maps (Fig. 1). In this study, a cut-off at 0.18 ms was performed (echoes at 0.06 ms and 0.12 ms were removed) for T_2 distribution calculation in order to isolate porewater signal from hydroxyls. Assuming that hydroxyls followed a monoexponential relaxation with a peak T_2 equal to 0.05 ms (from Fig. 1), only the exp(−0.18/

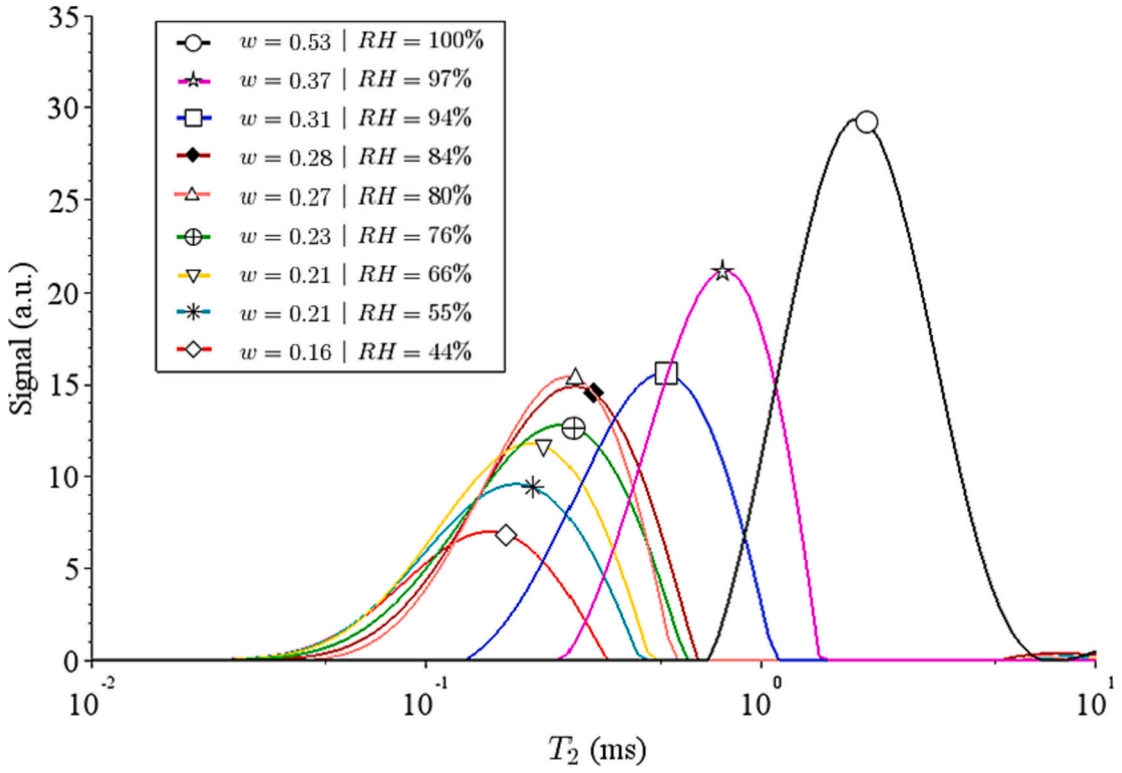

Fig. 3. T_2 distribution. The statistically most representative relaxation time of each peak (characteristic T_2) has been represented with a point symbol in the distribution.

0.05) = 2.7% of its signal could be detected. Single peak distributions were observed in all hydric states tested (Fig. 3). The peak at $RH = 44\%$ with relaxation times between 0.05 and 0.4 ms, shifted progressively towards larger values and larger signal intensities as RH increased until reaching 0.8–5 ms at $RH = 100\%$.

3.4. Characteristic T_1 and T_2

The statistically most representative relaxation times of each distribution peak of porewater, in the T_1-T_2 relaxation time maps and in the T_2 distribution (Figs. 1–3), were referred to as characteristic relaxation times (Table 2). They were calculated as the average for each T_1 or T_2 weighted by its corresponding NMR signal intensity. In T_1-T_2 relaxation time maps, closed contours are automatically detected by analyzing the local minimum. This enabled the identification of the porewater contour peak and the signal components relative to it, even considering overlap situations between two different contours.

T_1 slightly fluctuated in between 0.58 ms and 0.89 ms for samples at drier state (water content = 15.9–28.3%; RH = 44–84%). At wetter states, T_1 increased quickly with hydration and reached 2.87 ms at the saturated state. T_2 followed a similar trend, since it remained ranging between 0.17 ms and 0.39 ms for samples at the drier state and augmented quickly with hydration. At the saturated state, depending on the acquisition method, T_2 ranged between 1.74 and 2.35 ms.

3.5. Intensity of the NMR signal during hydration

The NMR signal measured is generally linearly proportional to the amount of water protons contained in the testing sample when using sequences as CPMG or IR. Verifying the linearity by reviewing the evolution of total signal intensity as a function of water content could provide an important assessment in order to verify whether all populations of water were measured. Quantification of the total signal intensity in the peaks of T_2 distribution (Fig. 3) required the calculation of the integral of the distribution, as the summation of signal intensity values from the start of the peak until its end. Peak areas were presented in arbitrary units multiplied by milliseconds (a.u. ms). In the case of T_1-T_2 map (Fig. 1), the signal intensity was calculated as the integral of the contour map exclusively from the porewater signal by the contour detection method described in Section 3.4, resulting in a peak volume with units (a.u. ms^2).

Results of peak area and peak volume (Fig. 4) highlighted that the evolution of total signal captured was linear with water content. Linear extrapolation suggested that samples prepared at water content lower content than 5% would not provide any NMR signal.

4. Interpretation and discussion

4.1. Relaxation time distribution in analysis of water absorption dynamic

T_1 and T_2 distributions and T_1-T_2 maps obtained in the present work (Fig. 1–3) showed a single peak pattern which progressively featured larger relaxation times, as observed in previous studies (Fleury et al., 2013; Ma et al., 2020; Tian et al., 2019; Tian and Wei, 2020; Sun et al., 2021). By the analysis of the evolution of the T_2 distribution during wetting or drying processes, notably its changes in shape and relaxation time, identification of hydration mechanisms is possible (Maillet et al., 2022). The shift towards higher relaxation times while maintaining distributions with similar shape during the wetting process could be identified by two mechanisms that may be coexisting: (i) storage of water on progressively larger saturated pore spaces. This mechanism proposes that hydration begins filling the smaller fraction of the porosity while the larger one can be totally dry. It is commonly used to explain capillary wetting processes; (ii) storage of water on the surface of unsaturated pore spaces that maintain constant the surface of water-solid contact throughout all the hydration process. The first mechanism could be attributed for instance to the adsorbed water in the interlayer spacing in montmorillonite and to the capillary water in general. The second mechanism might be attributed to adsorbed water surrounding the clay particles.

4.2. Two-regime hydration

4.2.1. Water retention curves

Water retention curves obtained from mixtures with contents of Na-bentonite ranging from 20 to 100% and different densities (Tang and Cui, 2010; Wang et al., 2013; Manca, 2015; Tian and Wei, 2020) are compared with this study (Fig. 5). Water content and effective dry density (ρ_{eff}) were calculated relative to the dry mass of montmorillonite (excluding the mass and volume of sand). Therefore, the sand fraction is

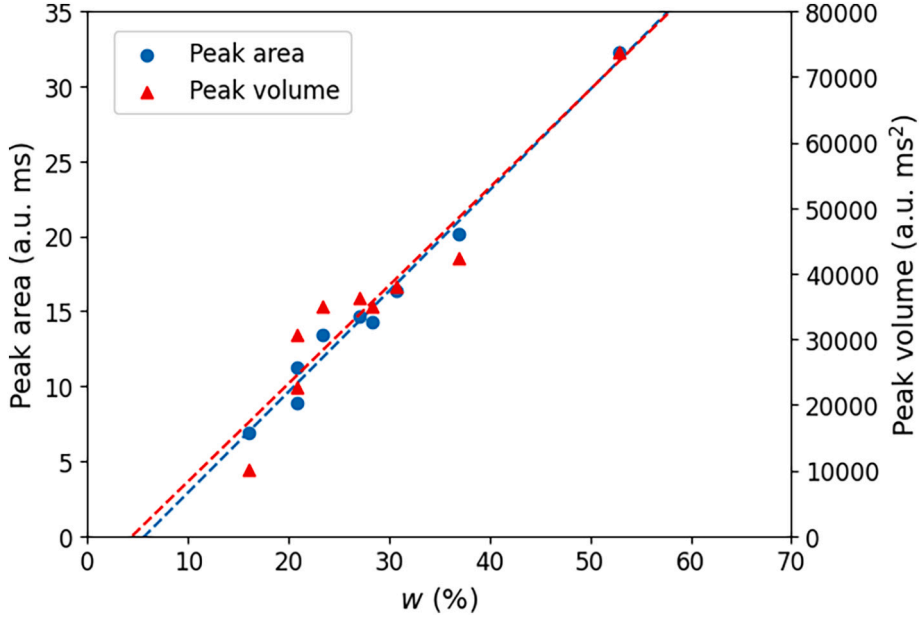

Fig. 4. Peak area and peak volume from the T_2 distributions and T_1-T_2 maps observed as a function of water content. Dashed line represents the linear fitting of the experimental data with an $R^2 = 0.9834$ (peak area) and $R^2 = 0.9206$ (peak volume).

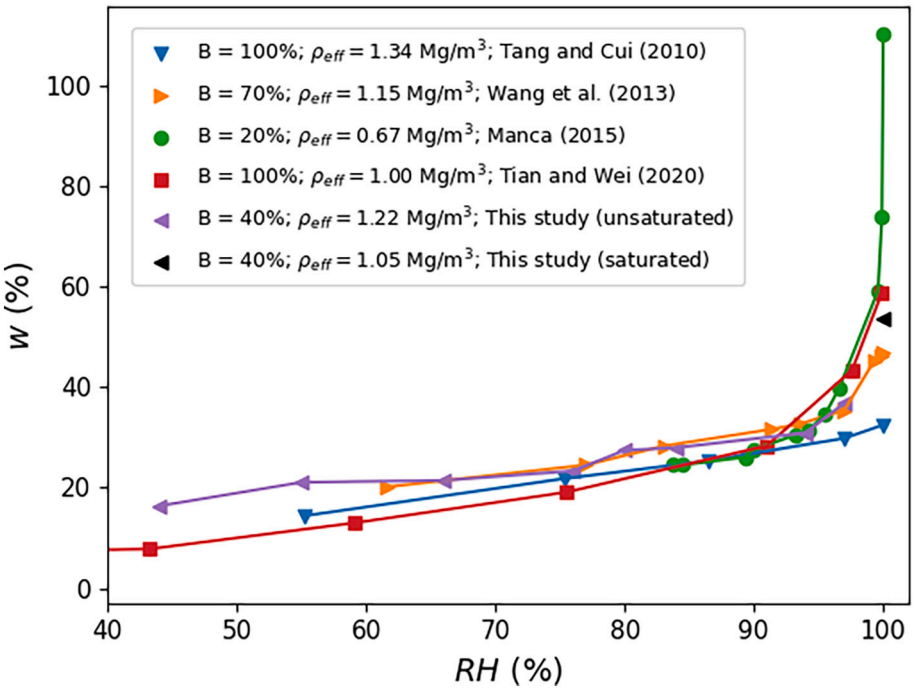

Fig. 5. Water retention curves of bentonite/sand mixtures containing bentonite fractions (*B*) ranging from 20% to 100% of their total dry mass. The effective dry density (ρ_{eff}) is calculated as the [(dry mass of clay minerals) / (total volume – sand volume)].

considered as an inert material which does not absorb any water. The reproductivity of water retention curves with different bentonite fractions highlights the dominant role of bentonite in the water absorption of the mixtures (Gray et al., 1984; Dixon et al., 1999; Komine, 2004).

A transition point in the hydration of bentonite was identified at high relative humidity (90–95%) corresponding to water contents of 29.8–32.8% in the studied mixture. This observation agrees with authors who determined the transition point at relative humidity values of 90–93% in confined bentonite (Lloret et al., 2003; Villar, 2005; Delage et al., 2006; Villar, 2007; Tang and Cui, 2010; Pintado et al., 2013). In the first regime, water content increases linearly with the relative humidity, where hydration takes place generally by adsorption onto the clay mineral surface due to the increasing concentration of water vapour in air. In the second regime, the evolution is no longer linear. It depends on the porosity of the sample given that the maximum water content reached at saturation state can be estimated by inferring the volume of

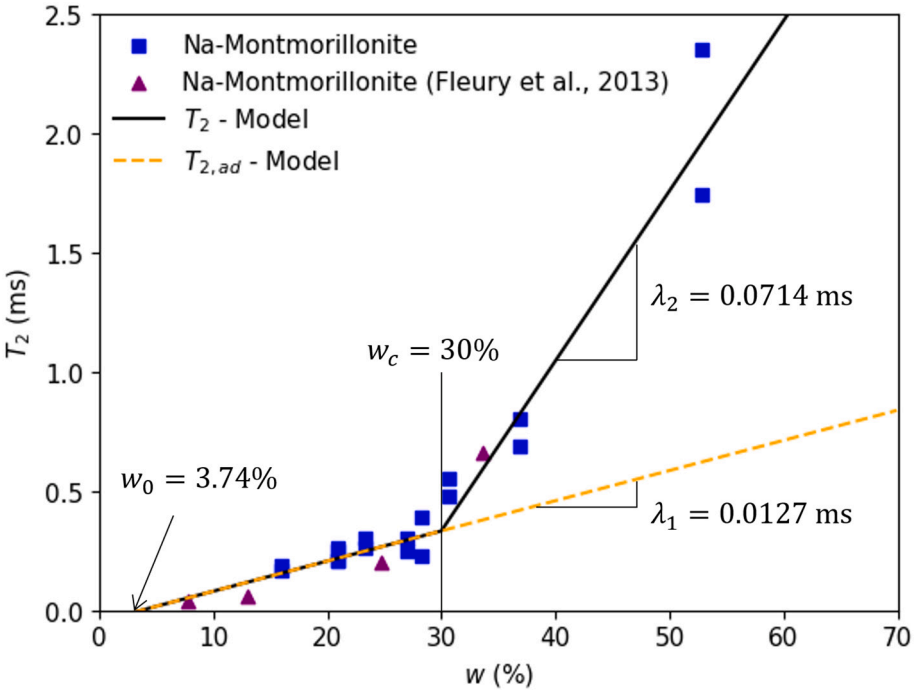

Fig. 6. Two-regime evolution of T_2 relaxation times from different wetting experiments in Na-montmorillonite. Estimations from the empirical model are plotted together with the experimental data.

water from the total volume of pores, for a given water density.

The water retention analysis described above is based on macroscopic observation. Contrast with microscopic experiments is required to prove the two-regime phenomena and provide an accurate transition point.

4.2.2. Relaxation times as a function of water content

Experimental data of the characteristic T_1 and T_2 evolution with hydration (Table 2) revealed that relaxation of porewater follows a slightly increasing regime at low relative humidity and a sharp increase at the higher hydration states ($w > 30\%$; $RH > 90\%$).

T_2 measurements (the most usual experimental measurement carried out in NMR relaxometry on expansive clays) are plotted together with data reported in works by Fleury et al. (2013) on Na-bentonite powder from Libya with 95% of montmorillonite content (Fig. 6). The evolution of T_2 confirms a transition point located at a water content of 30±1%, which corresponds to a relative humidity around 87–94% for a wide range of compacted mixtures of Na-bentonites from Wyoming (Fig. 5). Before the transition point, the linear increase has a slope of 0.0127 ms whereas at higher water contents the slope increases to 0.0714 ms (Fig. 6). The slopes were obtained by linear regression with a R^2 of 0.73 and 0.92 respectively.

The first regime is understood to be fully governed by the dynamics of the adsorbed water: linear dependence on water content, extremely fast T_2 below 0.40 ms, and the absence of capillary water. Overall mobility of adsorbed water could be linearly dependent on water content at low w and may explain the linear increase of T_2. In this regard, the osmotic adsorption of water at outer layers and the swelling of clay particles might decrease the overall clay surface-water interaction, even during the second regime.

The Na-bentonite powder used in Fleury et al. (2013) was not compacted and probably exhibited relatively low effective dry density. This can explain why relaxation times found in that material are predominantly lower. Nevertheless, the impact of effective dry density on relaxation times observed in saturated bentonite and bentonite/sand mixtures (Ohkubo et al., 2008; Eizaguirre et al., 2023) has not been proved at unsaturated conditions.

4.2.3. Empirical model for the two-regime evolution of T_2

To predict and interpret experimental data of T_2 evolution with water content, an empirical model, based on the distinction of two regimes with a transition point at a critical water content (w_c), is proposed following the observations of Section 4.2.2. T_2 values found in the first regime ($w \leq w_c$) correspond to the adsorbed water relaxation times ($T_{2,ad}$). The evolution of $T_{2,ad}$ is assumed linear with water content during both regimes. Therefore, $T_{2,ad}$ linear evolution features a slope λ_1 resulting from linear regression of T_2 experimental data in the first regime, which determines w_0 as the minimal water content that provides detectable relaxation times. T_2 and $T_{2,ad}$ are the same in the first regime. In the second regime T_2 is assumed to increase linearly with a slope λ_2 resulting from linear regression of T_2 experimental data in the second regime.

The relaxation times can thus be modeled (Fig. 6) by the Eqs. (2)–(3):

$$T_{2,ad} = \lambda_1 (w - w_0) \tag{2}$$

$$T_2 = \begin{cases} T_{2,ad} & if \ \ w \leq w_c \\ \lambda_2 (w - w_c) + \lambda_1 (w_c - w_0) & if \ \ w > w_c \end{cases} \tag{3}$$

4.3. Water content and NMR signal

Evaluating the total signal intensity (peak area and peak volume) (Fig. 4) given by the relaxation time distributions enables to verify empirically its proportionality with mass of water. For a known dry mass, total signal intensity enables deducing the water content by a non-destructive method, contrary to drying, after calibration with a known water mass-controlled sample measured under the same scanning parameters.

Fleury et al. (2022) quantified water content in 11 clay-rich sedimentary formations directly from CMPG sequences, highlighting in all specimens a close correlation with water content deduced from drying at 105 °C. For water contents lower than 10% linearity between signal intensity and water content was lost in Ningming clay, presumably due to the strong interaction between the water molecules and the surface of the different clay minerals, while below 5% of water content the NMR signal intensity became negligible (Ma et al., 2020). The close similitude with the findings obtained in the present work (Fig. 4) is remarkable even though this study did not test any sample below $w = 10\%$ and thus could not reproduce the linearity lost.

The empirical model presented in Section 4.2.3 (Fig. 6) predicts that in the case of Na-bentonite, at water contents of 5% approximately, the relaxation time would be low enough to have a distribution overlapping with the hydroxyls and therefore could not be quantified given that hydroxyls signal is systematically removed from the analysis as described in Sections 3.3–3.5.

4.4. Surface limited relaxation

In expansive clay, the mechanism governing the relaxation is attributed to the interaction between water protons and the solid surface of clay minerals. This relaxometry mechanism is known as surface limited relaxation (SLR) (Brownstein and Tarr, 1977; Godefroy et al., 2001). It assumes that after the induced NMR magnetic pulse, water protons can explore all the porewater space and get in contact with the pore wall undergoing a drastic relaxation of their magnetization. Therefore, the relaxation is fully dominated by the interaction of water molecules with the solid, in contrast to pure water in a very large pore where water molecules relax by diffusion without any appreciable solid surface perturbation. The SLR mechanism is usually attributed to small pore size media. Given the morphology of expansive clays (notably containing montmorillonite) which features a large specific surface area and very small pore sizes, this model is likely consistent to analyze relaxometry results. In addition, molecules of water travel by self-diffusion an approximate distance of $\sqrt{6\,D\,T_2} \approx 3$ µm during the relaxation process, where $D = 2.3 \cdot 10^{-9}$ (m^2/s) is the self-diffusion coefficient of pure water at 25 °C (Holz et al., 2000). Despite the approximations, this distance is presumably greater than the pore size where water is located when observing MIP pore size distribution evolution during wetting (Cui et al., 2002; Seiphoori et al., 2014).

4.4.1. Classical formulation

The SLR mechanism differentiate two populations of water in fast exchange: the porewater under the strong influence of the surface of the pore (surface population) with a volume, V_{surf}, and the bulk porewater (bulk population) with volume, V_{bulk}. The sum of both populations is the total porewater volume, V_w. The inverse of the characteristic relaxation time T_i (where i equals 1 or 2 for referring to longitudinal or transversal relaxation, respectively) is described in Eq. (4) as the inverse weighted average of the relaxation time featured in the surface population $T_{i,surf}$ and the relaxation time of the bulk population $T_{i,bulk}$, which is assumed to be 2300 ms at ambient temperature, similar to water in free state. Distinction of water densities for each water population is not considered in this expression. The $T_{i,bulk}$ term is orders of magnitude larger than the relaxation times found experimentally where $T_i \approx 1$ ms. Consequently, the bulk water term has a negligible contribution to T_i. Eq. (4) thus simplifies into Eq. (5). V_{surf} is usually decomposed into its thickness (ε) and its area, accessible via the specific surface area A_{ss} of the porous media. $T_{i,surf}$ and ε are directly related to the strength and electrochemical properties of the molecular interaction between the solid and the fluid. Several previous studies on expansive clays quantified the water-solid interaction with a parameter named surface relaxivity (ρ_i)

equals to $\varepsilon/T_{i,surf}$ (Guichet et al., 2008; Ohkubo et al., 2008, 2021; Tian and Wei, 2020). Given the surface relaxivity, it is possible to assess the volume of water and therefore the porosity in saturated conditions using Eq. (6).

$$\frac{1}{T_i} = \frac{1}{T_{i,bulk}} \frac{V_{bulk}}{V_w} + \frac{1}{T_{i,surf}} \frac{V_{surf}}{V_w} \tag{4}$$

$$T_i = T_{i,surf} \frac{V_w}{V_{surf}} \tag{5}$$

$$T_i = \frac{T_{i,surf}}{\varepsilon} \frac{V_w}{A_{ss}} = \frac{1}{\rho_i} \frac{V_w}{A_{ss}} \tag{6}$$

4.4.2. Proposed formulation

The expressions can be adapted to better represent the particular case of water mobility in expansive clays. In theory, SLR formulation corresponds to a weighted average accounting for the quantity of hydrogen protons (in water molecules) under the influence of the water-solid interface surface and those at bulk state. Therefore, a gravimetric weighted average expression (in terms of mass) is preferable to the volumetric weighted average expression in Eq. (4) which does not consider the variable density of porewater in clays. Additionally, the notion of adsorbed water population matches well with the definition given to the surface population (water molecules strongly influenced by the solid-water interaction). Therefore, the bulk population corresponds to the capillary water while the surface population refers to the adsorbed water, whose relaxation time is $T_{i,ad}$ equivalent to $T_{i,surf}$. In Eq. (7), m_w refers to the total mass of water, m_{ad} to the mass the adsorbed water and m_{bulk} to the mass of bulk water. As described in Section 4.4.1, the bulk water term can be neglected and following the separation of terms Eq. (8) is deduced. It describes for the first time a unique expression describing the evolution of the dual distribution of water populations (adsorbed and capillary water) directly from NMR relaxation times. Capillary water fraction is calculated as the complement to 100% of adsorbed water.

$$\frac{1}{T_i} = \frac{1}{T_{i,bulk}} \frac{m_{bulk}}{m_w} + \frac{1}{T_{i,ad}} \frac{m_{ad}}{m_w} \tag{7}$$

$$\frac{m_{ad}}{m_w} = \frac{T_{i,ad}}{T_i} \tag{8}$$

4.5. Application of the proposed model: Quantifying the adsorbed water fraction

Regarding Eq. 8, the characterization of two regimes separated at w_c = 30% as described in Section 4.2.2 would correspond to two regimes of water mobility. Applying the empirical model described in Section 4.2.3 to experimental data presented in Fig. 6, estimation of T_2 and $T_{2,ad}$ are provided for a wide range of water content. The model parameters were calculated from experimental data by linear regression fitting as described in Section 4.2.3. The value of w_c was set to 30% and the value of w_0 resulted to be 3.74%. Recent molecular simulations (Brochard, 2021) suggested that the first water layer in the interlayer space of montmorillonite would appear at $w < 7.5\%$ whereas the third layer at $26.2\% < w < 41.1\%$. Maybe the model parameters w_0 and w_c could have a physical sense related to the stepwise augmentation of basal spacing in montmorillonite.

Applying Eq. (8) with the model estimations of T_2 and $T_{2,ad}$ provide the proportion of adsorbed water as a function of water content (Fig. 7). The results highlight that the adsorbed water fraction constituted the 100% of water and then decreased sharply once the water content in the soil was above the transition point defined. For typical water contents at saturation state (higher than 40%) the decrease of adsorbed water begins to stabilize towards a value given by the ratio λ_1/λ_2 which may be only related to the clay mineral capacity to maintain the adsorption mechanism. Na-montmorillonite clays were tested but other type of clays would potentially fit the model.

Freezing experiments performed in Na-bentonite from Libya with 95% of montmorillonite content (Fleury et al., 2013) obtained that at RH = 11, 33 and 75% (w = 7.8, 12.9 and 24.7%) the totality of water was experiencing supercooling (thus, 100% adsorbed water) whereas at RH = 97% (w = 33.6%) the adsorbed water fraction was 73%. The

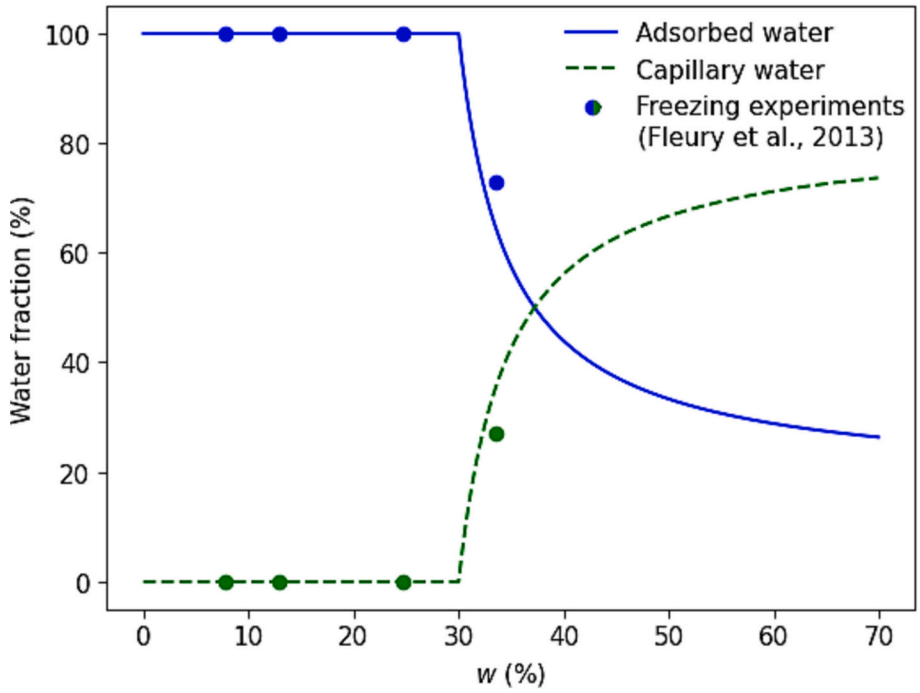

Fig. 7. Evolution of porewater populations in Na-montmorillonite as a function of water content using Eq. (8) with data of T_2 estimated with the empirical model. Points represent findings of freezing experiments (Fleury et al., 2013).

results of the model and the observations from freezing experiments fit remarkably well confirming the validity of the proposed model.

5. Conclusion and perspective

This study presented a complete range of experimental data on T_1 and T_2 relaxation times, performed on Na-bentonite/sand mixtures at various humidity-controlled conditions. T_1 distributions were not capable of representing porewater response due to the hydroxyl influence. To avoid it, a particular data treatment on T_1-T_2 maps and T_2 distribution was applied. The evolution of the most representative relaxation time of the T_2 distributions was investigated as a function of water content. A two-regime evolution was determined with a transition point at (w= 30%; RH = 90%) in accordance to the water retention curve transition point found. Both regimes featured linear progressions that were successfully identified and used to propose an empirical model able to reproduce the T_2 measurements on Na-montmorillonite regardless its effective dry density. At water contents lower than 5%, when no NMR signal is detected, the model suggested that T_2 was sufficiently fast to overlap its distribution with the hydroxyl signal not allowing its quantification.

A surface limited relaxation formulation was proposed in order to consider the particular case of expansive clays, introducing directly the adsorbed relaxation time into the equation. The formulation allowed the quantification of adsorbed water gravimetric fraction just from relaxation time data. Together with the empirical model, kinetics of adsorbed water and capillary water as a function of water content were successfully predicted, with a strong validation with experimental data. Water mobility would be very limited during a hydration process up until reaching *RH* of 90% when water behaviour would progressively change to capillary water provoking progressive increase on water mobility. The findings are a potential aide for the development of advanced water transport models. The impact of effective dry density on relaxation times observed in saturated bentonite-based mixtures (Ohkubo et al., 2008; Eizaguirre et al., 2023) requires to be proved at unsaturated conditions. It could illustrate the effect of compaction on water mobility and potentially redesign the proposed empirical model.

CRediT authorship contribution statement

Pablo Eizaguirre: Writing – original draft, Visualization, Methodology, Investigation, Formal analysis, Data curation, Conceptualization. **Anh Minh Tang:** Writing – original draft, Supervision, Resources, Project administration, Methodology, Conceptualization. **Benjamin Maillet:** Writing – review & editing, Supervision, Resources, Methodology, Formal analysis, Conceptualization. **Rahima Sidi-Boulenouar:** Supervision, Resources, Methodology, Conceptualization. **Jean Talandier:** Supervision, Resources, Project administration, Funding acquisition. **Jean-Michel Pereira:** Writing – review & editing, Supervision, Conceptualization. **Minh Ngoc Vu:** Supervision, Resources, Funding acquisition. **Baptiste Chabot:** Supervision, Resources, Methodology. **Patrick Dangla:** Supervision. **Michel Bornert:** Supervision. **Patrick Aimedieu:** Supervision.

Declaration of competing interest

The authors declare that they have no known competing financial interests or personal relationships that could have appeared to influence the work reported in this paper.

Data availability

Experimental data and data-treatment code are available on https://doi.org/10.57745/M4IVEE.

References

Bahramian, Y., Bahramian, A., Javadi, A., 2017. Confined fluids in clay interlayers: A simple method for density and abnormal pore pressure interpretation. Colloids Surf. A Physicochem. Eng. Asp. 521, 260–271. https://doi.org/10.1016/j.colsurfa.2016.08.021.

Brochard, L., 2021. Swelling of Montmorillonite from molecular simulations: hydration diagram and confined water properties. J. Phys. Chem. C 125, 15,527–15,543. https://doi.org/10.1021/acs.jpcc.1c02659.

Brownstein, K.R., Tarr, C.E., 1977. Spin-lattice relaxation in a system governed by diffusion. J. Magnet. Reson. 26, 17–24. https://doi.org/10.1016/0022-2364(77)90230-X.

Catinat, M., Fleury, M., Brigaud, B., Antics, M., Ungemach, P., 2023. Estimating permeability in a limestone geothermal reservoir from NMR laboratory experiments. Geothermics 111, 102,707. https://doi.org/10.1016/j.geothermics.2023.102707. , June.

Cui, Y., Loiseau, C., Delage, P., 2002. Microstructure changes of a confined swelling soil due to suction controlled hydration. In: Proceedings of the 3nd International Conference on Unsaturated Soils, UNSAT2002, pp. 593–598. Recife, Brazil.

Delage, P., Marcial, D., Cui, Y.J., Ruiz, X., 2006. Ageing effects in a compacted bentonite: a microstructure approach. Géotechnique 56, 291–304. https://doi.org/10.1680/geot.2006.56.5.291.

Dieudonne, A.C., Della Vecchia, G., Charlier, R., 2017. Water retention model for compacted bentonites. Can. Geotech. J. 54, 915–925. https://doi.org/10.1139/cgj-2016-0297.

Dixon, A., Graham, J., Gray, M.N., 1999. Hydraulic conductivity of clays in confined testsunder low hydraulic gradients. Can. Geotech. J. 36, 815–825. https://doi.org/10.1139/t99-057.

Eizaguirre, P., Tang, A.M., Maillet, B., Sidi-Boulenouar, R., Chabot, B., Bornert, M., et al., 2023. Impact of sand on the water retention properties of a bentonite/sand mixture by NMR characterization. (M. Bardanis, Éd.). E3S Web Conf. 382, 14,003. https://doi.org/10.1051/e3sconf/20233821400.

Faure, P.F., Rodts, S., 2008. Proton NMR relaxation as a probe for setting cement pastes. Magn. Reson. Imaging 26, 1183–1196. https://doi.org/10.1016/j.mri.2008.01.026.

Fleury, M., Kohler, E., Norrant, F., Gautier, S., M'Hamdi, J., Barré, L., 2013. Characterization and Quantification of Water in Smectites with Low-Field NMR. J. Phys. Chem. C 117, 4551–4560. https://doi.org/10.1021/jp311006q.

Fleury, M., Gimmi, T., Mazurek, M., 2022. Porewater content, pore structure and water mobility in clays and shales from NMR methods. Clay Clay Miner. 70, 417–437. https://doi.org/10.1007/s42860-022-00195-4.

Gao, H., Li, H., 2015. Determination of movable fluid percentage and movable fluid porosity in ultra-low permeability sandstone using nuclear magnetic resonance (NMR) technique. J. Pet. Sci. Eng. 133, 258–267. https://doi.org/10.1016/j.petrol.2015.06.017.

Gens, A., Guimaraes, L.N., Garcia-Molina, A., Alonso, E.E., 2002. Factors controlling rock–clay buffer interaction in a radioactive waste repository. Eng. Geol. 64, 297–308. https://doi.org/10.1016/S0013-7952(02)00026-1.

Godefroy, S., Korb, J.-P., Fleury, M., Bryant, R.G., 2001. Surface nuclear magnetic relaxation and dynamics of water and oil in macroporous media. Phys. Rev. E 64, 021605. https://doi.org/10.1103/PhysRevE.64.021605.

Gray, M.N., Cheung, S.C.H., Dixon, D.A., 1984. The influence of sand content on swelling pressures and structure developed in statically compacted Na-bentonite (AECL–7825). Canada. https://inis.iaea.org/search/search.aspx?orig_q=RN:16054988.

Guichet, X., Fleury, M., Kohler, E., 2008. Effect of clay aggregation on water diffusivity using low field NMR. J. Colloid Interface Sci. 327, 84–93. https://doi.org/10.1016/j.jcis.2008.08.013.

Holz, M., Heil, S.R., Sacco, A., 2000. Temperature-dependent self-diffusion coefficients of water and six selected molecular liquids for calibration in accurate ^{1}H NMR PFG measurements. Phys. Chem. Chem. Phys. 2, 4740–4742. https://doi.org/10.1039/b005319h.

Jacinto, A.C., Villar, M.V., Ledesma, A., 2012. Influence of water density on the water-retention curve of expansive clays. Géotechnique 62, 657–667. https://doi.org/10.1680/geot.7.00127.

Jaeger, F., Bowe, S., Van As, H., Schaumann, G.E., 2009. Evaluation of ^{1}H NMR relaxometry for the assessment of pore-size distribution in soil samples. Eur. J. Soil Sci. 60, 1052–1064. https://doi.org/10.1111/j.1365-2389.2009.01192.x.

Karnland, O., Olsson, S., Nilsson, U., 2006. Mineralogy and sealing properties of various bentonites and smectite-rich clay materials. SKB TR-06-30, Sweden. https://www.osti.gov/etdeweb/servlets/purl/922488.pdf.

Komine, H., 2004. Simplified evaluation on hydraulic conductivities of sand–bentonite mixture backfill. Appl. Clay Sci. 26, 13–19. https://doi.org/10.1016/j.clay.2003.09.006.

Lebeau, M., Konrad, J.-M., 2010. A new capillary and thin film flow model for predicting the hydraulic conductivity of unsaturated porous media. Water Resour. Res. 46 https://doi.org/10.1029/2010WR009092, 2010WR009092.

Leroy, P., Revil, A., 2004. A triple-layer model of the surface electrochemical properties of clay minerals. J. Colloid Interface Sci. 270, 371–380. https://doi.org/10.1016/j.jcis.2003.08.007.

Lloret, A., Villar, M.V., Sánchez, M., Gens, A., Pintado, X., Alonso, E.E., 2003. Mechanical behaviour of heavily compacted bentonite under high suction changes. Géotechnique (1), 27–40. https://doi.org/10.1680/geot.2003.53.1.27.

Low, P.F., 1961. In: Norman, A.G. (Ed.), Physical Chemistry of Clay-Water Interaction, 13, pp. 269–327. https://doi.org/10.1016/S0065-2113(08)60962-1.

Ma, T., Wei, C., Yao, C., Yi, P., 2020. Microstructural evolution of expansive clay during drying–wetting cycle. Acta Geotech. 15, 2355–2366. https://doi.org/10.1007/s11440-020-00938-4.

Madsen, F.T., Müller-Vonmoos, M., 1989. The swelling behaviour of clays. Appl. Clay Sci. 4, 143–156. https://doi.org/10.1016/0169-1317(89)90005-7.

Maillet, B., Sidi-Boulenouar, R., Coussot, P., 2022. Dynamic NMR relaxometry as a simple tool for measuring liquid transfers and characterizing surface and structure evolution in porous media. Langmuir 38, 15,009–15,025. https://doi.org/10.1021/acs.langmuir.2c01918.

Martin, R.T., 1960. Adsorbed water on clay: a review. Clays Clay Miner. 9, 28–70. https://doi.org/10.1016/B978-1-4831-9842-2.50007-9.

Manca, D., 2015. Hydro-chemo-mechanical characterization of sand/bentonite mixtures, with a focus on the water and gas transport properties.

Mitchell, J.K., Soga, K., 2005. Fundamentals of Soil Behaviour, 3rd ed. John Wiley & Sons, Hoboken.

Muurinen, A., Carlsson, T., Root, A., 2013. Bentonite pore distribution based on SAXS, chloride exclusion and NMR studies. Clay Miner. 48, 251–266. https://doi.org/10.1180/claymin.2013.048.2.07.

Navarro, V., Asensio, L., De la Morena, G., Pintado, X., Yustres, Á., 2015. Differentiated intra- and inter-aggregate water content models of mx-80 bentonite. Appl. Clay Sci. 118, 325–336. https://doi.org/10.1016/j.clay.2015.10.015.

Navarro, V., Cabrera, V., Merlo, O., De la Morena, G., Torres-Serra, J., 2022. Density of water adsorbed on bentonites: Determination and effect on microstructural void ratio modelling. Appl. Clay Sci. 219, 106,434. https://doi.org/10.1016/j.clay.2022.106434.

Ohkubo, T., Kikuchi, H., Yamaguchi, M., 2008. An approach of NMR relaxometry for understanding water in saturated compacted bentonite. Phys. Chem. Earth Parts A/B/C 33, S169–S176. https://doi.org/10.1016/j.pce.2008.10.042.

Ohkubo, T., Yamazaki, A., Fukatsu, Y., Tachi, Y., 2021. Pore distribution of compacted Ca-montmorillonite using NMR relaxometry and cryoporometry: Comparison with Na-montmorillonite. Microporous Mesoporous Mater. 313, 110,841. https://doi.org/10.1016/j.micromeso.2020.110841. , January.

Penvern, H., Zhou, M., Maillet, B., Courtier-Murias, D., Scheel, M., Perrin, J., et al., 2020. How Bound Water Regulates Wood Drying? Phys. Rev. Appl. 14, 054051 https://doi.org/10.1103/PhysRevApplied.14.054051.

Pintado, X., Mamunul, H.M., Martikainen, J., 2013. Thermo-hydro-mechanical tests of buffer material (POSIVA–12-49). Finland. https://inis.iaea.org/collection/NCLCollectionStore/_Public/45/087/45087749.pdf.

Provencher, S.W., 1982. A constrained regularization method for inverting data represented by linear algebraic or integral equations. Comput. Phys. Commun. 27, 213–227. https://doi.org/10.1016/0010-4655(82)90173-4.

Revil, A., Lu, N., 2013. Unified water isotherms for clayey porous materials: Unified Water Isotherm. Water Resour. Res. 49, 5685–5699. https://doi.org/10.1002/wrcr.20426.

Rongwei, S., Tsukahara, T., 2020. Effect of cations on interlayer water dynamics in cation-exchanged montmorillonites studied by nuclear magnetic resonance and x-ray diffraction techniques. ACS Earth Space Chem. 4, 535–544. https://doi.org/10.1021/acsearthspacechem.9b00315.

Seiphoori, A., Ferrari, A., Laloui, L., 2014. Water retention behaviour and microstructural evolution of MX-80 bentonite during wetting and drying cycles. Géotechnique 64, 721–734. https://doi.org/10.1680/geot.14.P.017.

Sellin, P., Leupin, O.X., 2013. The use of clay as an engineered barrier in radioactive-waste management – a review. Clay Clay Miner. 61, 477–498. https://doi.org/10.1346/CCMN.2013.0610601.

Sun, Y., Jiang, S., Li, S., Wang, X., Peng, S., 2021. Hydrate formation from clay bound water for CO2 storage. Chem. Eng. J. 406, 126,872. https://doi.org/10.1016/j.cej.2020.126872.

Tang, A.M., Cui, Y.J., 2010. Effects of mineralogy on thermo-hydro-mechanical parameters of MX80 bentonite. J. Rock Mech. Geotech. Eng. 2 (1), 91–96. https://doi.org/10.3724/SP.J.1235.2010.00091.

Tang, A.-M., Cui, Y.-J., 2005. Controlling suction by the vapour equilibrium technique at different temperatures and its application in determining the water retention properties of MX80 clay. Can. Geotech. J. 42, 287–296. https://doi.org/10.1139/t04-082.

Tian, H.H., Wei, C.F., 2020. Characterization and Quantification of Pore Water in Clays During Drying Process With Low-Field NMR. Water Resour. Res. 56 https://doi.org/10.1029/2020WR027537 e2020WR027537.

Tian, H., Wei, C., Yan, R., 2019. Thermal and saline effect on mineral-water interactions in compacted clays: A NMR-based study. Appl. Clay Sci. 170, 106–113. https://doi.org/10.1016/j.clay.2019.01.015.

Tian, H., Wu, G., Wei, C., 2023. An NMR-Based Procedure for Evaluating the Apparent SurfaceRelaxivity and Pore Size Distribution of Soils. Geotech. Test. J. 47 (3) https://doi.org/10.1520/GTJ20230395.

Tuller, M., Or, D., 2005. Water films and scaling of soil characteristic curves at low water contents: scaling of characteristic curves. Water Resour. Res. 41 https://doi.org/10.1029/2005WR004142.

Tuller, M., Or, D., Dudley, L.M., 1999. Adsorption and capillary condensation in porous media: Liquid retention and interfacial configurations in angular pores. Water Resour. Res. 35, 1949–1964. https://doi.org/10.1029/1999WR900098.

Villar, M.V., 2005, July. MX-80 Bentonite. Thermo-Hydro-Mechanical characterization performed at CIEMAT in the context of the Prototype Project. Spain. https://inis.iaea.org/collection/NCLCollectionStore/_Public/36/083/36083408.pdf.

Villar, M., 2007. Water retention of two natural compacted bentonites. Clay Clay Miner. (55), 311–322. https://doi.org/10.1346/CCMN.2007.0550307.

Wang, Q., Tang, A.M., Cui, Y.-J., Delage, P., Barnichon, J.-D., Ye, W.-M., 2013. The effects of technological voids on the hydro-mechanical behaviour of compacted bentonite–sand mixture. Soils Found. 53, 232–245. https://doi.org/10.1016/j.sandf.2013.02.004.

Wang, H., Shirakawabe, T., Komine, H., Ito, D., Gotoh, T., Ichikawa, Y., Chen, Q., 2020. Movement of water in compacted bentonite and its relation with swelling pressure. Can. Geotech. J. 57, 921–932. https://doi.org/10.1139/cgj-2019-0219.

Wersin, P., Curti, E., Appelo, C.A., 2004. Modelling bentonite–water interactions at high solid/liquid ratios: swelling and diffuse double layer effects. Appl. Clay Sci. 26, 249–257. https://doi.org/10.1016/j.clay.2003.12.010.